**Atmospheric
Chemistry
and Physics
Discussions**

ACPD

6, 7051–7073, 2006

Nanoparticle phase
transitions

G. Biskos et al.

Title Page

Abstract	Introduction
Conclusions	References
Tables	Figures

◄◄   ►►

◄   ►

Back   Close

Full Screen / Esc

Printer-friendly Version

Interactive Discussion

EGU

Prompt deliquescence and efflorescence of aerosol nanoparticles

G. Biskos[1], D. Paulsen[1], L. M. Russell[2], P. R. Buseck[3], and S. T. Martin[1]

[1]Division of Engineering and Applied Sciences, Harvard University, Cambridge, MA 02138, USA
[2]Scripps Institution of Oceanography, University of California San Diego, La Jolla, CA 92093, USA
[3]Departments of Geological Sciences and Chemistry/Biochemistry, Arizona State University, Tempe, AZ 85287, USA

Correspondence to: S. T. Martin (scot_martin@harvard.edu)

Abstract

Literature reports have differed on the possibilities of discontinuous and continuous (i.e., prompt and nonprompt) deliquescence and efflorescence of aerosol particles in the nanosize regime. Experiments reported herein using a hygroscopic tandem nano-differential mobility analyzer demonstrate prompt deliquescence and efflorescence of ammonium sulfate particles having diameters from 6 to 60 nm. Apparent nonprompt-ness can be induced both by operation of the experimental apparatus and by interpretation of the measurements, even though the underlying phase transitions of individual particles remain prompt. No nanosize effect on the relative humidity values of deliquescence or efflorescence is observed for the studied size range. Smaller hygroscopic growth factors are, however, observed for the nanoparticles, in agreement with thermodynamic calculations that include the Kelvin effect. A slightly nonspherical shape for dry ammonium sulfate particles is inferred from their hygroscopically induced reconstruction between 5 and 30% relative humidity. Our results provide a further understanding of nanoparticle behavior, especially relevant to the growth rates of atmospheric nanoparticles.

1 Introduction

Despite their small mass, the chemical composition of atmospheric aerosol nanoparticles can now be determined in part due to recent advances in analytical instrumentation (McMurry, 2000). Observations employing this instrumentation indicate that freshly nucleated ambient particles having diameters of a few nanometers are frequently composed primarily of ammonium and sulfate ions at variable mixing ratios (Kulmala et al., 2004). For example, aerosol mass spectra recorded during new-particle nucleation events in Pittsburgh (September 2002) showed that particles having diameters from 18 to 33 nm were mainly composed of sulfuric acid (Zhang et al., 2004). Hygroscopic growth factors of 25-nm particles following a nucleation event in Gosan, Korea

EGU

EGU

(April 2001), were similar to those of laboratory-generated ammonium sulfate particles (Buzorius et al., 2004). Mass spectra recorded for particles from 6 to 15 nm during nucleation events in Atlanta (August 2002) showed that ammonium sulfate accounted for the entire sampled nanoparticle mass (Smith et al., 2005). Concurrent measurements of the hygroscopic growth factors were also consistent with ammonium sulfate (Sakurai et al., 2005).

Ammonium sulfate nanoparticles form in the atmosphere by homogeneous nucleation in the presence of gas-phase sulfuric acid, water, and ammonia (Ball et al., 1999). Once formed, the freshly nucleated particles grow, through processes of condensation and coagulation, to diameters large enough to become optically active. During the growth process, a principal factor affecting the condensation and coagulation rates is particle hygroscopicity because physical state (i.e., solid or liquid) and particle diameter vary with relative humidity (RH). Once large enough to be optically active, the particles influence the radiative properties of the atmosphere and thus directly the climate of the Earth at regional and global scales. The larger particles also indirectly affect the Earth's climate through their action on cloud formation.

The hygroscopic behavior of nanoparticles can be different from that of their large-particle counterparts because the relative contribution of the surface term to the free energy of a particle increases markedly for sub-100 nm particles (Chen, 1994; Mirabel et al., 2000; Djikaev et al., 2001; Russell and Ming, 2002; Biskos et al., 2006a). Sodium chloride nanoparticles have been investigated most thoroughly. One effect is that the deliquescence and efflorescence relative humidity values (hereafter, DRH and ERH, respectively) of sodium chloride particles increase for mobility diameters smaller than 40 nm (Hämeri et al., 2001; Biskos et al., 2006a). A second effect is that the hygroscopic growth factor of the sodium chloride nanoparticles decreases because of the Kelvin effect (Hämeri et al., 2001), although quantitative agreement between predictions and observations must also take into account a size-dependent shape factor in the Knudsen regime (Biskos et al., 2006b).

Measurements of the hygroscopic properties of ammonium sulfate nanoparticles

have also been made, and intermediate growth factors were observed for RH values around the DRH (Hämeri et al., 2000). The results led Mirabel et al. (2000) in a theory paper to introduce the concepts of prompt and nonprompt deliquescence. Prompt deliquescence corresponds to a discontinuous increase of particle diameter during the phase transition that accompanies increasing RH, whereas nonprompt deliquescence refers to continuous growth. Mirabel et al. (2000) hypothesized that nanosized particles have nonprompt behavior in contrast to the prompt behavior of their large-particle counterparts (e.g., as observed in the large-particle experiments of Cohen et al., 1987; Tang and Munkelwitz, 1994; Weis and Ewing, 1996; Cziczo et al., 1997; Onasch et al., 1999; Wise et al., 2005). Djikaev et al. (2001) subsequently modeled the deliquescence process for nanosized particles and reported an absence of nonprompt behavior. In further modeling papers, Russell and Ming (2002) and Topping et al. (2005) also predicted that prompt deliquescence of nanoparticles should occur. In this paper, we provide fresh experimental results to show that both deliquescence and efflorescence of ammonium sulfate nanoparticles are prompt and that the earlier data of Hämeri et al. (2000), which has been interpreted to support nonprompt deliquescence, can instead be reproduced by an artifact tied to the operation of the experimental apparatus.

2 Experimental

A hygroscopic tandem nano-differential mobility analyzer (TnDMA) was employed to study the deliquescence, the efflorescence, and the hygroscopic growth of monodisperse ammonium sulfate particles having mobility diameters from 6 to 60 nm. Experiments were carried out in duplicate for particles generated both by electrospray and by atomization to test for any influence of preparation method on the results (e.g., possible chemical impurities enriched in nanoparticles).

The electrospray aerosol generator (TSI Model 3480) employed 10- and 100-mM aqueous solutions of ammonium sulfate (EMD Chemical Inc., 99.5% purity) for nanoparticles of 6–20 nm and 40–60 nm mobility diameter, respectively. High-purity

water (Barnstead Model D8971; 18 MΩ cm) for the solutions was prepared by consecutive steps including filtration, ultraviolet irradiation, and reverse osmosis. The primary aerosol particles exiting the 40-μm capillary tube of the electrospray generator were diluted with 2 Lpm filtered dry air, resulting in an aerosol stream of below 0.1% RH. The aerosols had lognormal particle number size distributions. From the 10-mM solution, the mode diameter was 10 nm, the geometric standard deviation was 1.3, and the integrated particle number concentration was 10^6 cm^{-3}. The respective quantities for the 100-mM solution were 15 nm, 1.6, and 6×10^6 cm^{-3}.

An atomizer (TSI Model 3076) was also used to generate aerosol samples. A 0.1 wt% solution was atomized in N$_2$, following a method similar to that of Hämeri et al. (2000). The polydisperse aerosol was dried to below 10% RH by mixing with dry air and passing through a diffusion dryer (TSI Model 3062). The mode diameter of the lognormal particle number size distribution was 15 nm, the geometric standard deviation was 1.4, and the integrated particle number concentration was 4×10^6 cm^{-3}.

Figure 1 shows a schematic layout of the TnDMA used in the experiments. A description of an earlier version of the apparatus was provided in Biskos et al. (2006a). In brief, the polydisperse aerosol particles were passed through a ^{85}Kr neutralizer (TSI Model 3077) and a first nano-DMA (TSI Model 3085). The resulting monodisperse particles were then exposed to an RH history through a series of one or two single-tube Nafion humidity exchangers (Perma Pure Model MD-110), after which their number size distribution was measured with a second nano-DMA and an ultrafine CPC (TSI Model 3025). The RH history allowed either deliquescence- or efflorescence-mode experiments to be carried out. For instance, in deliquescence mode, the RH history of the aerosol prior to a number-size-distribution measurement was 5%→X%, where X was increased stepwise as the independent variable of an experiment (i.e., X=RH$_a$ of Fig. 1). In efflorescence mode, the RH history prior to a number-size-distribution measurement was 5%→95%→X%.

Modifications to the system described by Biskos et al. (2006a) were as follows. DMA-2 employed closed-loop recirculation for the sheath flow instead of the open-flow cir-

culation. This change somewhat improved the precision of replicate experiments by ensuring that the sheath flow-in was exactly balanced by the sheath flow-out. The re-circulation setup depicted in Fig. 1 employed a blower (Minispiral Model SE12RE21SA) that collected the excess flow from the DMA and drove it through (1) a hydrophobic filter (Whatman Model 6702-7500) to remove particles, (2) a heat exchanger (Lytron Model C-HX-4105G1SB) to equilibrate the temperature (heated by 2–3 K in the compressive blower), (3) a laminar flow element (Furness Controls Model FCO96-20) coupled to a pressure transducer (Aschroft Model CXLdp) and a proportional-integral-derivative (PID) controller (Omega Model CNI16D52-C24-DC) to provide feedback to the blower speed and thereby control the flow rate, and (4) a multiple-tube Nafion conditioner (Permapure Model PD-50T) to rapidly adjust the relative humidity to the desired value. The flow then reentered the DMA as the sheath flow, which was regularly calibrated by use of a Gilibrator bubble flow meter. In the usual mode of operation, we set the relative humidity of the sheath flow (RH_s) equal to the relative humidity of the aerosol (i.e., $RH_s = RH_a$) by opening valve C and closing valve D. For specific experiments de-signed to compare our results with those of Hämeri et al. (2000), we closed valve C and opened valve D and then set $RH_s = RH_a + 3\%$ by using an independent RH generator (cf. Fig. 1). We employed 1.5 Lpm for the aerosol flow and 15 Lpm for the sheath flow at 6-nm mobility diameter and steadily decreased the respective flows for increasing mobility diameter, i.e., 0.3 Lpm and 5 Lpm at 60-nm mobility diameter.

3 Results and discussion

The results of a deliquescence-mode experiment are shown in Fig. 2 for particles having a 10-nm dry mobility diameter. The number size distributions show that deli-quescence occurs at 79±2.5% RH, which is consistent with the large-particle value of 79.5% (cf. Martin, 2000). Apparent differences in the deliquescence relative humidity (e.g., 79% in Fig. 2a and 80% in Fig. 2b) lie within the day-to-day variability of the pre-cision of the RH measurements. The hygroscopic responses for particles generated

by electrospray and atomization are similar.

Provided that $RH_s = RH_a$, there is a prompt phase change for a 1% increase in RH from a mode centered at 10 nm to one centered at 13 nm following deliquescence (Figs. 2a and b). In some measurements, two separate peaks, which correspond to aqueous and solid particles, are observed for RH_a close to DRH. This effect arises from slight heterogeneities of relative humidity in the apparatus. Once the particles are aqueous above 80% RH, further increase of the RH results in water condensation and, therefore, additional diameter growth.

For $RH_s = RH_a + 3\%$, which follows the protocol of Hämeri et al. (2000), there is an apparent nonprompt phase change: the apparent mode diameter increases continuously from 10.3 nm at 76% RH, to 10.7 nm at 78% RH, to 11.2 nm at 79% RH, to 12.5 nm at 81% RH (Fig. 2c). Contrary to the experiments in which $RH_s = RH_a$, no distinct peaks that correspond to the two phases of the particles (i.e., solid and aqueous) are observed. The size distribution, however, widens for 78 and 79% RH. This apparent nonpromptness does not reflect the true particle behavior but rather is an artifact of the experimental method and analysis, as next explained.

The apparent nonprompt deliquescence occurs for $RH_s = RH_a + 3\%$ because the particles deliquesce within DMA-2. There is a slow equilibration of the RH between the laminar aerosol and sheath flows, arising from diffusive and limited convective mixing during transport through the DMA classification column. For instance, consider $RH_s = 80\%$ and $RH_a = 77\%$ when the flows enter the DMA. The particles in the aerosol flow are not immediately exposed to 80% RH when the aerosol and sheath flows merge at the top of the classification column. Rather, after traveling some distance in the classification column as solid particles of smaller mobility diameter, they abruptly deliquesce to form aqueous particles of increased mobility diameter. The classified particles emerging from the DMA therefore have an apparent mobility diameter that is a weighted-average of their transport time as solid and aqueous particles. Mikhailov et al. (2004; Fig. 14 therein) reported a similar effect in their study of 100-nm sodium chloride particles. Numerical modeling by us of air flow and diffusive-convective RH mixing

is consistent with deliquescence during particle transport inside the DMA (model not discussed further herein).

This RH mixing effect inside the DMA leads to the observation of a smoothly increasing growth factor. As the RH values of the sample and sheath flows increase during a scan (e.g., $RH_s=81\%$ and $RH_a=78\%$), deliquescence occurs further upstream in the classification column, and the weighted-averaged apparent mobility diameter increases. According to this explanation, the underlying deliquescence events are prompt, and the apparent nonpromptness results, as an artifact, from these abrupt deliquescence events occurring inside the classification column. This explanation rules out our earlier hypothesis (Biskos et al., 2006a, b) that impurities concentrated by atomization could explain literature reports of nonprompt deliquescence of nanoparticles. Furthermore, the apparent widening of the distribution from 77 to 79% RH (Fig. 2c) can be explained by small RH variations in the flow field, causing some particles to deliquesce earlier and some later along their paths within the DMA.

Efflorescence-mode experiments for particles having a 10-nm dry mobility diameter show an apparent nonprompt behavior even for $RH_s=RH_a$ (Fig. 3). Here, the explanation for apparent nonpromptness differs from that provided above for the deliquescence-mode experiments. In efflorescence mode, the mean mobility diameter of the aqueous particles decreases for decreasing RH, which is explained by the evaporation of water that accompanies reversible hygroscopic growth. For RH>35%, the observations show that the decrease of mobility diameter with RH (i.e., $d'_m=\mathrm{d}d_m/\mathrm{d}RH$) proceeds rather gently and in agreement with quantitative predictions (see Appendix concerning the hygroscopic growth factor). For 34 to 31% RH, however, d'_m increases greatly and diverges from predictions. At 30% RH, d'_m abruptly goes to zero, indicating that crystallization is complete. These measurements could erroneously be interpreted to suggest that particle crystallization for $RH_s=RH_a$ is nonprompt because no abrupt shift of narrow, distinct peaks is observed during the RH scan from 35 to 30%. The increase both of the width of the size distribution from 34 to 31% RH and of d'_m over this same range, however, indicates that a different explanation is correct: there are

EGU

two overlapping, incompletely resolved modes corresponding to solid and aqueous particles.

This explanation can be developed further, as follows. For 10-nm dry mobility-diameter particles of ammonium sulfate, the hygroscopic growth factor at 34% RH is 1.075 (see Appendix and also Fig. 4). For the typical operating conditions of DMA-1 (i.e., an aerosol-to-sheath flow ratio of 1:10), the size distribution of the monodisperse aerosol has a one-sigma geometric standard deviation (gsd) of 1.04. The data for 34% RH in Fig. 3 are successfully fit by two Gaussian peaks having gsd's of 1.04 and a geometric mode separation of 1.07. The existence of two modes in the efflorescence data across 3% RH (i.e., 34 to 31% RH), compared to across just 1% RH for the deliquescence data, arises from either greater RH gradients for lower RH values in the NCA (Fig. 1) or stochastic nucleation and crystallization of individual aerosol particles during the residence time in the apparatus (Martin, 2000).

The hygroscopic behavior of 10-nm dry mobility-diameter particles is summarized in Fig. 4, including a comparison to the results of Hämeri et al. (2000). The points in Fig. 4 correspond to the mode diameters of the fits to the deliquescence and efflorescence data. For $RH_s = RH_a$, prompt deliquescence occurs for both the electrosprayed and the atomized particles (upper right panel). For $RH_s = RH_a + 3\%$, however, intermediate growth factors are recorded because deliquescence occurs within the classification column. The results of Hämeri et al. (2000), also recorded using $RH_s = RH_a + 3\%$, are in qualitative agreement with this nonprompt trend. The efflorescence points in the bottom panel of Fig. 4 are shown for a one-peak fit to the data (i.e., apparent nonprompt efflorescence); the efflorescence points in the upper left panel correspond to solid- and aqueous-modes of a two-peak fit to the data for 31%<RH<34% (cf. discussion of Fig. 3).

The slope of the intermediate growth factors depends on several instrumental factors. For instance, an increasing difference between RH_a and RH_s decreases the slope further. Likewise, the RH mixing rate within DMA-2 is affected both by the design of the DMA and the flow rates through it. Sizing of larger particles typically implies

lower flow rates and therefore longer residence times of the particles in the classifier, allowing deliquescence closer to the DMA entrance. Two designs of Hauke-type DMA's (namely, one for particles smaller than 30 nm and another for those larger than 30 nm) are employed by Hämeri et al. (2000). In comparison, a TSI nano-DMA is used in our
5   apparatus. These factors provide a possible explanation for the difference in the extent of nonpromptness between the results reported in this study (red circles in Fig. 4) and those in Hämeri et al. (2000) (black open diamonds). Differences in the design and the operating conditions of the DMA's may explain another observation in Hämeri et al. (2000) that 15- and 30-nm particles appear to have a more prompt deliquescence
10 than 8- and 10-nm particles (cf. Fig. 2 therein).

The hygroscopic behavior for 6- to 60-nm dry mobility-diameter particles generated by electrospray is summarized in Figure 5, including a comparison to model predictions of hygroscopicity. For fixed relative humidity, the hygroscopic growth of nanoparticles decreases with decreasing particle size. For example, the mobility-diameter growth
15 factor at 80% RH is 1.22 for 6-nm particles compared to 1.44 for 60-nm particles. For comparison, for sodium chloride particles the analogous values are 1.51 and 1.77, respectively (Biskos et al., 2006b). The model predictions in Fig. 5 differ on whether the Kelvin effect is included or not (see Appendix). The measurements agree within 4% with the model predictions that include the Kelvin effect. This agreement suggests
20 that the physical parameters used in the calculations (i.e., the surface tension, the density of the aqueous particles, the density of the dry particles, and the relationship of activity to weight percent composition) are known accurately enough to predict the hygroscopic growth of ammonium sulfate nanoparticles. Even so, there appears to be a systematic bias of 1 to 2% in the comparisons between the model predictions and
25 the measurements, with slightly greater bias for decreasing particle size.

The small systematic bias between the model predictions and the measurements can be explained by a shape factor correction of 1.02, thus implying slightly nonspherical particles. This explanation is corroborated by the decrease of the growth factor during deliquescence-mode experiments from 1.00 for RH<5% to 0.99 to 0.98 for

EGU

EGU

20%<RH<60% (Fig. 6). This decrease in mobility diameter, most evident for particles smaller than 10 nm, arises from changes in particle shape and is driven by restructuring to more stable forms. The implication is that the mobility diameter for RH<5% is 1 to 2% larger than the volume-equivalent diameter, so that the observed growth

5　factors are systematically 1 to 2% smaller than the predicted growth factors. (The increase in growth factor between 65 and 80% RH arises from adsorbed layers of water; Romakkaniemi et al., 2001.)

The data in Fig. 5 show that there is no nanosize effect on the deliquescence relative humidity (79.5%) or the efflorescence relative humidity (35%) of ammonium sulfate.

10　This conclusion is subject to the caveats of the size range investigated (6 to 60 nm), the experimental uncertainty (2.5% in RH and 1 to 2% in mobility diameter), the time allowed for a phase transition (between 1 and 2 s), and the particle preparation methods employed. The data of Hämeri et al. (2000) also suggest an absence of a nanosize effect provided that the DRH value is taken at the median growth factor of the nonprompt

15　observations. The experimental observations of an absence of a nanosize effect on DRH disagree with theoretical predictions, which have hypothesized based upon assumed physical parameters that the DRH should increase for decreasing particle size (Chen, 1994; Russell and Ming, 2002; Topping et al., 2005).

The absence in the experimental observations of a nanosize effect for the deliques-

20　cence and efflorescence phase transitions of ammonium sulfate differs from the presence of an effect for sodium chloride, for which deliquescence shifts from 75% for large particles to 87% RH for a 6-nm particle and efflorescence from 45% to 53% for a similar change in particle size (Biskos et al., 2006b). A possible implication is that the surface properties of ammonium sulfate differ from those of sodium chloride.

25　In conclusion, the measurements presented in this paper show that deliquescence and efflorescence of ammonium sulfate nanoparticles are prompt, similarly to their large-particle counterparts. Earlier reports of nonprompt deliquescence are explained by the operating conditions of the DMA and the interpretation of the data. There is no discernable nanosize effect on the deliquescence and efflorescence relative humidity

values of ammonium sulfate particles, in contrast to the phase transitions of sodium chloride nanoparticles. The hygroscopic growth factors observed for ammonium sulfate nanoparticles agree with thermodynamic predictions that take into account the Kelvin effect. An accurate description of the hygroscopic behavior of nanoparticles, including their phase transitions and growth factors, is a foundational component of accurate models of nucleation and growth processes of atmospheric nanoparticles.

Supporting information available

The data shown in Figs. 2 to 6 are available electronically (http://www.atmos-chem-phys-discuss.net/6/7051/2006/acpd-6-7051-2006-supplement.zip).

Appendix A

Description of models 1 and 2

The mobility-diameter growth factor g is calculated from the measurements as follows:

$$g(\text{RH}) = \frac{d_m(\text{RH})}{d_{m,\text{dry}}}, \tag{A1}$$

where $d_{m,\text{dry}}$ is the mobility diameter of the dry particle (viz. RH<5%) and $d_m(\text{RH})$ is the mobility diameter at increased relative humidity. Literature accounts suggest that submicron dry ammonium sulfate particles are nearly spherical and, therefore, have a shape factor χ of 1.00 (Zelenyuk et al., 2006). The restructuring shown in Fig. 6 for increasing RH, however, demonstrates that shape factor differs slightly from 1.00 (e.g., 1.02; see further discussion in main text). The following development of the models nevertheless assumes that the dry ammonium sulfate particles have

EGU

a unity shape factor, in which case $d_{m,\mathrm{dry}}=d_{ve,\mathrm{dry}}$ where d_{ve} denotes the volume-equivalent diameter. After deliquescence, the aqueous particles are also spherical, implying that $d_m(\mathrm{RH})=d_{ve}(\mathrm{RH})$. For these conditions, Eq. (A1) then simplifies to $g(\mathrm{RH})=d_{ve}(\mathrm{RH})/d_{ve,\mathrm{dry}}$. (For development of the case $\chi\neq1.00$, see Biskos et al., 2006b).

We consider two models of the mobility-diameter growth factor: the first omits the Kelvin effect and the second includes it (Biskos et al., 2006a). Omission of the Kelvin effect implies that $a_w=\mathrm{RH}/100$ for model 1, where a_w is the water activity in the aqueous particles. Model 1 is described by the following equation:

$$g(\mathrm{RH}) = \frac{d_{ve}(\mathrm{RH})}{d_{ve,\mathrm{dry}}} = \left(\frac{100\,\rho_s}{w_t(a_w)\,\rho(w_t(a_w))}\right)^{1/3}, \tag{A2}$$

where ρ_s is the density of the dry particle, $\rho(w_t(a_w))$ is the density of the aqueous solution droplet, and $w_t(a_w)$ is the weight percent of solute in the aqueous particle. Equations for these quantities are given in Table 1.

Model 2 expands on model 1 by including the Kelvin effect, which relates RH to a_w as follows:

$$\mathrm{RH} = 100\,a_w \exp\left(\frac{4M_w\,\sigma_{aq}(w_t(a_w))}{RT\rho_w\,d_{ve}(\mathrm{RH})}\right), \tag{A3}$$

where ρ_w is the density of pure water, $\sigma_{aq}(w_t(a_w))$ is the surface tension of the aqueous droplet (Table 1), M_w is the molar mass of water, R is the universal gas constant, and T is the temperature. Model 2 predicts $g(\mathrm{RH})$ by solving for $d_{ve}(\mathrm{RH})$ and $a_w(\mathrm{RH})$ that simultaneously satisfy Eqs. (A2) and (A3).

Plots of $g(\mathrm{RH})$ based on models 1 and 2 are shown in Figure 5 as the solid and dot-dashed lines, respectively.

Nanoparticle phase transitions

G. Biskos et al.

References

Ball, S. M., Hanson, D. R., Eisele, F. L., and McMurry, P. H.: Laboratory studies of particle nucleation: Initial results for H_2SO_4, H_2O, and NH_3 vapors, J. Geophys. Res., 104, 23 709–23 718, 1999.

Biskos, G., Malinowski, A., Russell, L. M., Buseck, P. R., and Martin, S. T.: Nanosize effect on the deliquescence and the efflorescence of sodium chloride particles, Aerosol Sci. Technol., 40, 97–106, 2006a.

Biskos, G., Russell, L. M., Buseck, P. R., and Martin, S. T.: Nanosize effect on the hygroscopic growth factor of aerosol particles, Geophys. Res. Lett., 33, L07801, doi:10.1029/2005GL025199, 2006b.

Buzorius, G., McNaughton, C. S., Clarke, A. D., Covert, D. S., Blomquist, B., Nielsen, K., and Brechtel, F. J.: Secondary aerosol formation in continental outflow conditions during ACE-Asia, J. Geophys. Res., 109, D24203, doi:10.1029/2004JD004749, 2004.

Chen, J. P.: Theory of deliquescence and modified Köhler curves, J. Atmos. Sci., 51, 3505–3516, 1994.

Cohen, M. D., Flagan, R. C., and Seinfeld, J. H.: Studies of concentrated electrolyte solutions using the electrodynamic balance. 1. Water activities for single-electrolyte solutions, J. Phys. Chem., 91, 4563–4574, 1987.

Cziczo, D. J., Nowak, J. B., Hu, J. H., and Abbatt, J. D. P.: Infrared spectroscopy of model tropospheric aerosols as a function of relative humidity: Observation of deliquescence and crystallization, J. Geophys. Res., 102, 18 843–18 850, 1997.

Djikaev, Y. S., Bowles, R., Reiss, H., Hameri, K., Laaksonen, A., and Vakeva, M.: Theory of size dependent deliquescence of nanoparticles: Relation to heterogeneous nucleation and comparison with experiments, J. Phys. Chem. B, 105, 7708–7722, 2001.

Hämeri, K., Laaksonen, A., Väkevä, M., and Suni, T.: Hygroscopic growth of ultrafine sodium chloride particles, J. Geophys. Res., 106, 20 749–20 757, 2001.

Hämeri, K., Väkevä, M., Hanson, H.-C., and Laaksonen, A.: Hygroscopic growth of ultrafine

EGU

ammonium sulphate aerosol measured using an ultrafine tandem differential mobility analyzer, J. Geophys. Res., 105, 22 231–22 242, 2000.

Kulmala, M., Vehkamaki, H., Petajda, T., Dal Maso, M., Lauri, A., Kerminen, V. M., Birmili, W., and McMurry, P. H.: Formation and growth rates of ultrafine atmospheric particles: a review of observations, J. Aerosol Sci., 35, 143–176, 2004.

Martin, S. T.: Phase transitions of aqueous atmospheric particles, Chem. Rev., 100, 3403–3453, 2000.

McMurry, P. H.: A review of atmospheric aerosol measurements, Atmos. Environ., 34, 1959–1999, 2000.

Mikhailov, E., Vlasenko, S., Niessner, R., and Pöschl, U.: Interaction of aerosol particles composed of protein and salts with water vapor: hygroscopic growth and microstructural rearrangement, Atmos. Chem. Phys., 4, 323–350, 2004.

Mirabel, P., Reiss, H., and Bowles, R. K.: A theory for the deliquescence of small particles, J. Chem. Phys., 113, 8200–8205, 2000.

Onasch, T. B., Siefert, R. L., Brooks, S. D., Prenni, A. J., Murray, B., Wilson, M. A., and Tolbert, M. A.: Infrared spectroscopic study of the deliquescence and efflorescence of ammonium sulfate aerosol as a function of temperature, J. Geophys. Res., 104, 21 317–21 326, 1999.

Perry, R. H. and Green, D. W.: Perry's Chemical Engineers' Handbook, McGraw Hill, New York, 1997.

Pruppacher, H. R. and Klett, J. D.: Microphysics of Clouds and Precipitation, Kluwer Academic Publishers, Boston, 1997.

Romakkaniemi, S., Hameri, K., Vakeva, M., and Laaksonen, A.: Adsorption of water on 8–15 nm NaCl and $(NH_4)_2SO_4$ aerosols measured using an ultrafine tandem differential mobility analyzer, J. Phys. Chem. A, 105, 8183–8188, 2001.

Russell, L. M. and Ming, Y.: Deliquescence of small particles, J. Chem. Phys., 116, 311–321, 2002.

Sakurai, H., Fink, M. A., McMurry, P. H., Mauldin, L., Moore, K. F., Smith, J. N., and Eisele, F. L.: Hygroscopicity and volatility of 4–10 nm particles during summertime atmospheric nucleation events in urban Atlanta, J. Geophys. Res., 110, D22S04, doi:10.1029/2005JD005918, 2005.

Smith, J. N., Moore, K. F., Eisele, F. L., Voisin, D., Ghimire, A. K., Sakurai, H., and McMurry, P. H.: Chemical composition of atmospheric nanoparticles during nucleation events in Atlanta, J. Geophys. Res., 110, D22S03, doi:10.1029/2005JD005912, 2005.

Tang, I. N. and Munkelwitz, H. R.: Aerosol phase-transformation and growth in the atmosphere,

Nanoparticle phase transitions

G. Biskos et al.

Title Page

Abstract	Introduction
Conclusions	References
Tables	Figures

◄ | ►

◄ | ►

Back | Close

Full Screen / Esc

Printer-friendly Version

Interactive Discussion

EGU

J. Appl. Meteorol., 33, 791–796, 1994.

Tang, I. N., Tridico, A. C., and Fung, K. H.: Thermodynamic and optical properties of sea salt aerosols, J. Geophys. Res., 102, 23 269–23 275, 1997.

Topping, D. O., McFiggans, G. B., and Coe, H.: A curved multi-component aerosol hygroscopicity model framework: Part 1 – Inorganic compounds, Atmos. Chem. Phys., 5, 1205–1222, 2005.

Weis, D. D. and Ewing, G. E.: Infrared spectroscopic signatures of $(NH_4)_2SO_4$ aerosols, J. Geophys. Res., 101, 18 709–18 720, 1996.

Wise, M. E., Biskos, G., Martin, S. T., Russell, L. M., and Buseck, P. R.: Phase transitions of single salt particles studied using a transmission electron microscope with an environmental cell, Aerosol Sci. Technol., 39, 849–856, 2005.

Zelenyuk, A., Cai, Y., and Imre, D.: From agglomerates of spheres to irregularly shaped particles: Determination of dynamic shape factors from measurements of mobility and vacuum aerodynamic diameters, Aerosol Sci. Technol., 40, 197–217, 2006.

Zhang, Q., Stanier, C. O., Canagaratna, M. R., Jayner, J. T., Wornsnop, D. R., Pandis, S. N., and Jimenez, J. L.: Insights into the chemistry of new particle formation and growth events in Pittsburgh based on aerosol mass spectrometry, Env. Sci. Technol., 38, 4797–4809, 2004.

Nanoparticle phase transitions

G. Biskos et al.

EGU

Table 1. Density ρ (kg m^{-3}), water activity a_w, and surface tension σ_{aq} (N m^{-1}) of ammonium sulfate for $0 < w_t < 78\%$. Data sources: ρ_s (Perry and Green, 1997), ρ_{aq} and a_w (Tang et al., 1997), and σ_{aq} (Pruppacher and Klett, 1997).

$$\rho_s = 1770$$
$$\rho_{aq} = 997.1 + \sum A_i w_t^i \qquad A_1 = 5.920$$
$$A_2 = -5.036 \times 10^{-3}$$
$$A_3 = 1.024 \times 10^{-5}$$
$$a_w = 1.0 + \sum C_i w_t^i \qquad C_1 = -2.715 \times 10^{-3}$$
$$C_2 = 3.113 \times 10^{-5}$$
$$C_3 = -2.336 \times 10^{-6}$$
$$C_4 = 1.412 \times 10^{-8}$$
$$\sigma_{aq} = 0.072 + \frac{0.0234\, w_t}{100 - w_t}$$
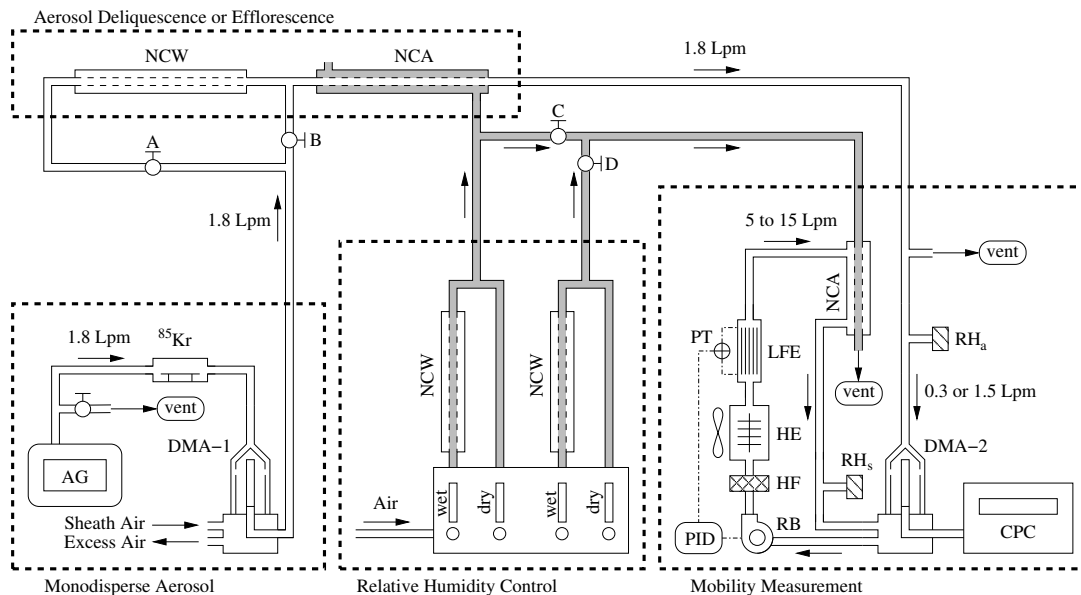
Fig. 1. Schematic layout of the tandem nano-DMA. Key: AG, aerosol generator (electrospray or atomizer); [85]Kr, Krypton source aerosol neutralizer; DMA, differential mobility analyzer; CPC, condensation particle counter; LFE, laminar flow element; HE, heat exchanger; HF, high efficiency particulate air (HEPA) filter; PID, proportional-integral-derivative controller; PT, pressure transducer; RB, recirculation blower; NCA, Nafion conditioner with air; NCW, Nafion conditioner with water; RH_s, sheath-flow relative-humidity monitor of DMA-2; and RH_a, aerosol-flow relative-humidity monitor of DMA-2. Vent is connected to the house hood. Filtered dry house air is used for the sheath flow of DMA-1 and for the relative humidity control. In a deliquescence-mode experiment, valve A is closed and valve B is open. In an efflorescence-mode experiment, valve A is open and valve B is closed. Valve C is open and valve D is closed to set $RH_s = RH_a$. For independent values of RH_s and RH_a (e.g., $RH_s = RH_a + 3\%$), valve C is closed and valve D is open. Gray and clear paths denote gas and aerosol flows, respectively. See Biskos et al. (2006a) for further description of the elements in this figure.

EGU

(a) Electrospray Deliquescence for $RH_s = RH_a$

(b) Atomization Deliquescence for $RH_s = RH_a$

(c) Electrospray Deliquescence for $RH_s = RH_a + 3\%$

Normalized Concentration

Mobility Diameter (nm)
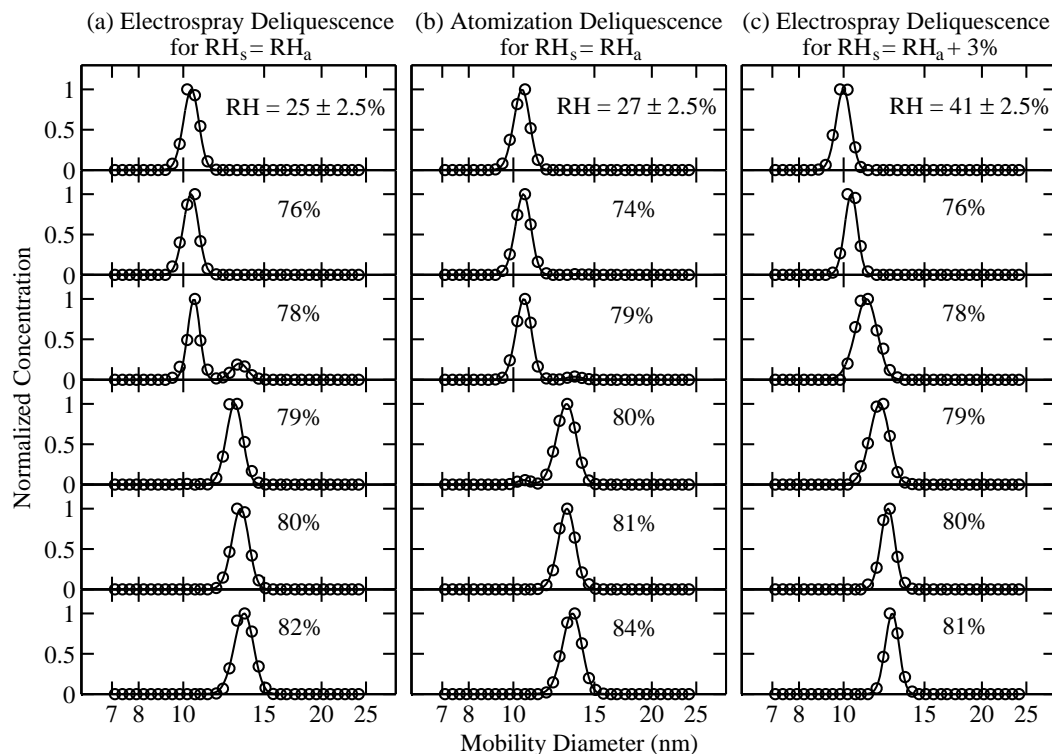
Fig. 2. Deliquescence-mode measurements of ammonium sulfate aerosol particles generated by electrospray or atomization. The RH history in each measurement is 5%→X%, where X is the value given in each panel. Measured (circles) and fitted (solid lines; one-peak Gaussian function) number size distributions are shown for increasing RH. In a and b, the RH of the sheath flow equals that of the aerosol flow. In c, the RH of the sheath flow is +3% compared to that of the aerosol flow (Hämeri et al., 2000). Temperature is 298 K. The dry mobility diameter is 10 nm.
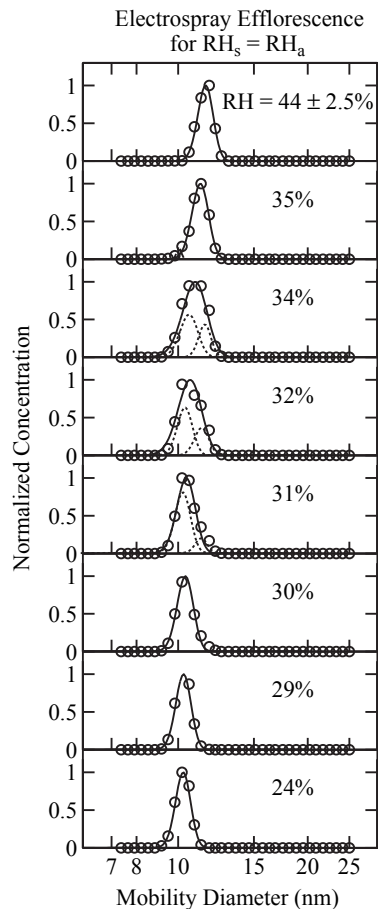
Fig. 3. Efflorescence-mode measurements of ammonium sulfate aerosol particles generated by electrospray. The RH history in each measurement is 5%→95%→X%, where X is the RH value given in each panel. Measured (circles) and fitted (solid lines) number size distributions are shown for decreasing RH. At 32 and 34% RH, the apparent widening of the number size distributions arises from overlapping peaks of dry and aqueous aerosol particles, which are resolved by the two-peak Gaussian fit shown in the figure (dashed lines). Temperature is 298 K. The dry mobility diameter is 10 nm.
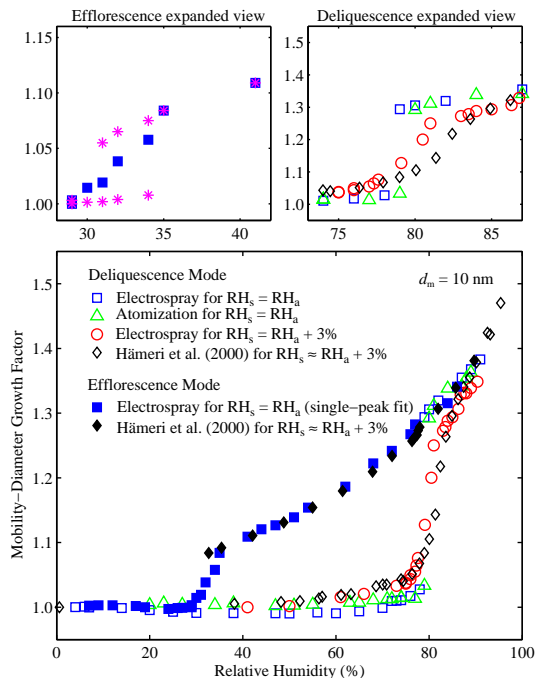
Fig. 4. Hygroscopic growth curves showing that prompt deliquescence and efflorescence occur provided that $RH_s = RH_a$ (cf. caption to Fig. 2). Temperature is 298 K. The dry mobility diameter is 10 nm. The ordinate values are calculated from the measurements (e.g., Figs. 2 and 3) using Eq. (A1). Solid symbols were recorded during efflorescence-mode experiments, and open symbols were recorded during deliquescence-mode measurements. Diamonds show the data of Hämeri et al. (2000), for which $RH_s \approx RH_a + 3\%$. The upper panels show expanded views of the efflorescence-mode data from 30 to 40% RH (left panel) and the deliquescence-mode data from 75 to 85% RH (right panel). The solid blue points in the main and upper panels show the efflorescence data analyzed using a one-peak fit whereas the solid magenta points in the upper panel show the data analyzed using a two-peak fit of overlapping dry and aqueous modes (cf. Fig. 3).

EGU
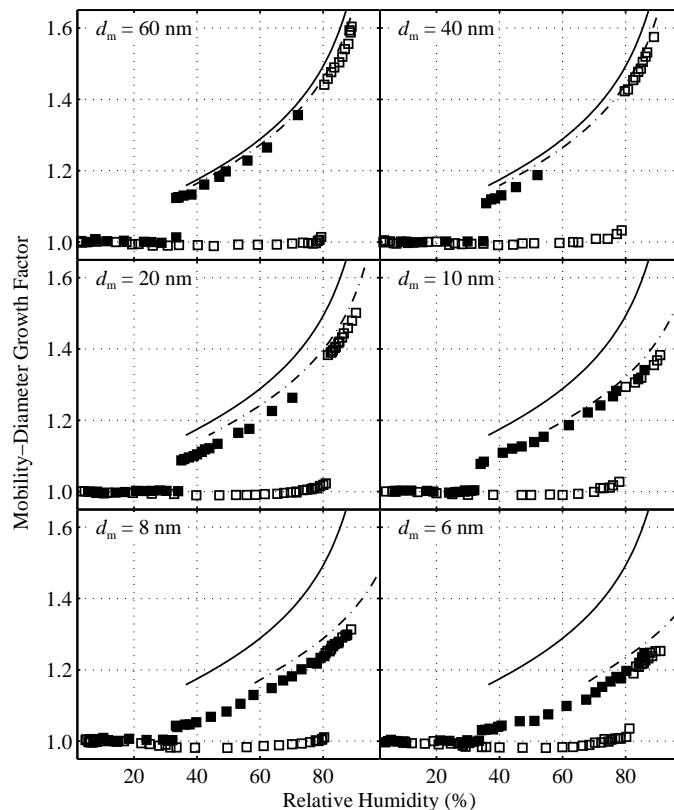
Fig. 5. Hygroscopic growth curves of ammonium sulphate aerosol particles generated by electrospray. Open symbols were recorded during deliquescence-mode measurements. Solid symbols were recorded during efflorescence-mode experiments and were analyzed by using either one- or two-peak fits, as necessary (cf. Figs. 3 and 4). Lines show the growth factors of models that omit (solid line) and include (dot-dashed line) the Kelvin effect (viz. models 1 and 2 described in the Appendix). Models are evaluated for $0 < w_t < 78\%$.
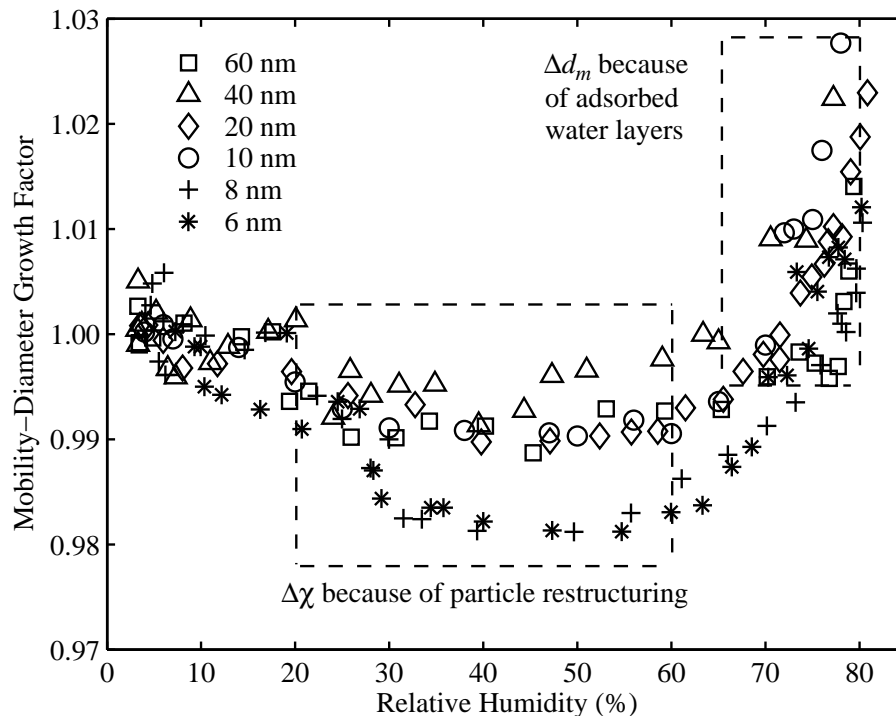
Fig. 6. Comparison at intermediate RH values (i.e., below DRH) of the hygroscopic growth factors g of ammonium sulfate aerosol particles of 6- to 60-nm mobility diameter during deliquescence-mode experiments. Particles are generated by electrospray. Equation (A1) provides the definition of g(RH). Between 20 and 60% RH, g(RH) decreases because the particle shape factor χ(RH) decreases (i.e., approaching spherical shape). Between 65 and 80% RH, g(RH) increases because adsorbed water layers increase the mobility diameter d_m(RH). The RH history of the particles is 5%→X%, where X is the abscissa value. The observations do not change for an RH history that includes a pre-treatment step of 5%→90%→5%→X% (data not shown), in contrast to the behavior of sodium chloride particles (Biskos et al., 2006b). For all the measurements, RH$_a$=RH$_s$.

Title Page

Abstract | Introduction

Conclusions | References

Tables | Figures

|◄ | ►|

◄ | ►

Back | Close

Full Screen / Esc

Printer-friendly Version

Interactive Discussion

EGU